

Ultra-high sensitivity of multicolor Sm³⁺-doped LiSrVO₄ phosphors for contactless optical thermometer

Peng Du*, Yafei Hou, Weiping Li, Laihui Luo*

^aDepartment of Microelectronic Science and Engineering, School of Physical Science and Technology, Ningbo University, 315211 Ningbo, Zhejiang, China

Corresponding author: dp2007good@sina.com or dupeng@nbu.edu.cn (P. Du);
luolaihui@nbu.edu.cn (L. Luo)

Table S1. CIE coordinates and CCT values of the LiSrVO₄:xSm³⁺ phosphors as a function of Sm³⁺ ion concentration.

Compounds	CIE coordinates		CCT
	<i>x</i>	<i>y</i>	
LiSrVO ₄	0.374	0.470	4578 K
LiSrVO ₄ :0.005Sm ³⁺	0.437	0.446	3303 K
LiSrVO ₄ :0.01Sm ³⁺	0.449	0.447	3124 K
LiSrVO ₄ :0.03Sm ³⁺	0.464	0.434	2818 K
LiSrVO ₄ :0.05Sm ³⁺	0.469	0.428	2706 K
LiSrVO ₄ :0.07Sm ³⁺	0.469	0.422	2661 K

Table S2. CIE coordinates of the $\text{LiSrVO}_4:0.01\text{Sm}^{3+}$ phosphors as a function of temperature.

Compounds	Temperature	CIE coordinates	
		x	y
$\text{LiSrVO}_4:0.01\text{Sm}^{3+}$	303 K	0.449	0.447
$\text{LiSrVO}_4:0.01\text{Sm}^{3+}$	313 K	0.462	0.430
$\text{LiSrVO}_4:0.01\text{Sm}^{3+}$	323 K	0.476	0.423
$\text{LiSrVO}_4:0.01\text{Sm}^{3+}$	333 K	0.490	0.414
$\text{LiSrVO}_4:0.01\text{Sm}^{3+}$	343 K	0.504	0.408
$\text{LiSrVO}_4:0.01\text{Sm}^{3+}$	353 K	0.517	0.402
$\text{LiSrVO}_4:0.01\text{Sm}^{3+}$	363 K	0.529	0.398
$\text{LiSrVO}_4:0.01\text{Sm}^{3+}$	373 K	0.539	0.394
$\text{LiSrVO}_4:0.01\text{Sm}^{3+}$	383 K	0.548	0.392

Table S3. Maximum S_a and S_r values of the $\text{LiSrVO}_4:0.005\text{Sm}^{3+}$, $\text{LiSrVO}_4:0.01\text{Sm}^{3+}$ and $\text{LiSrVO}_4:0.05\text{Sm}^{3+}$ phosphors.

Compounds	S_a	S_r
$\text{LiSrVO}_4:0.005\text{Sm}^{3+}$	0.071 K ⁻¹	2.253% K ⁻¹
$\text{LiSrVO}_4:0.01\text{Sm}^{3+}$	1.076 K ⁻¹	6.167% K ⁻¹
$\text{LiSrVO}_4:0.05\text{Sm}^{3+}$	0.048 K ⁻¹	1.394% K ⁻¹

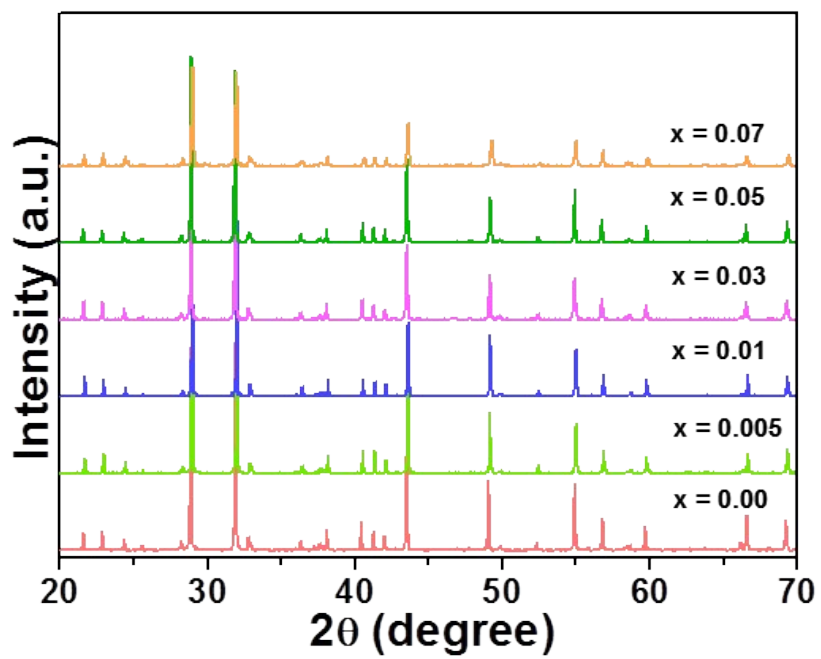


Figure S1 XRD patterns of the $\text{LiSrVO}_4:x\text{Sm}^{3+}$ phosphors as a function of Sm^{3+} ion content.

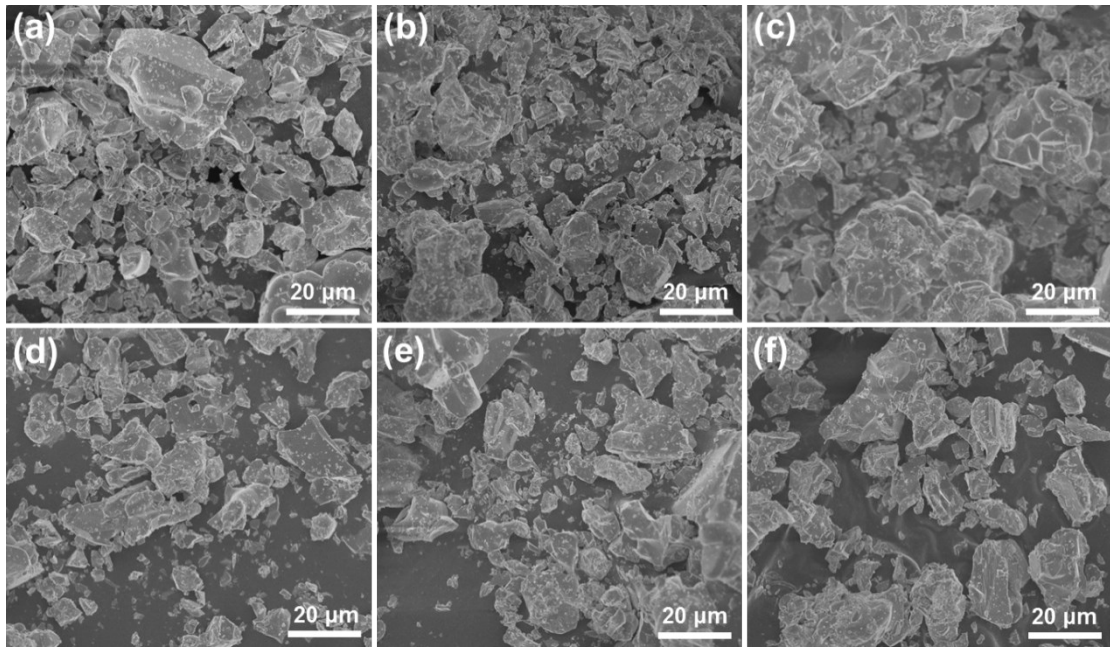


Figure S2. FE-SEM images of $\text{LiSrVO}_4\text{:}x\text{Sm}^{3+}$ (a) $x = 0.00$, (b) $x = 0.005$, (c) $x = 0.01$, (d) $x = 0.03$, (e) $x = 0.05$ and (f) $x = 0.07$ phosphors.

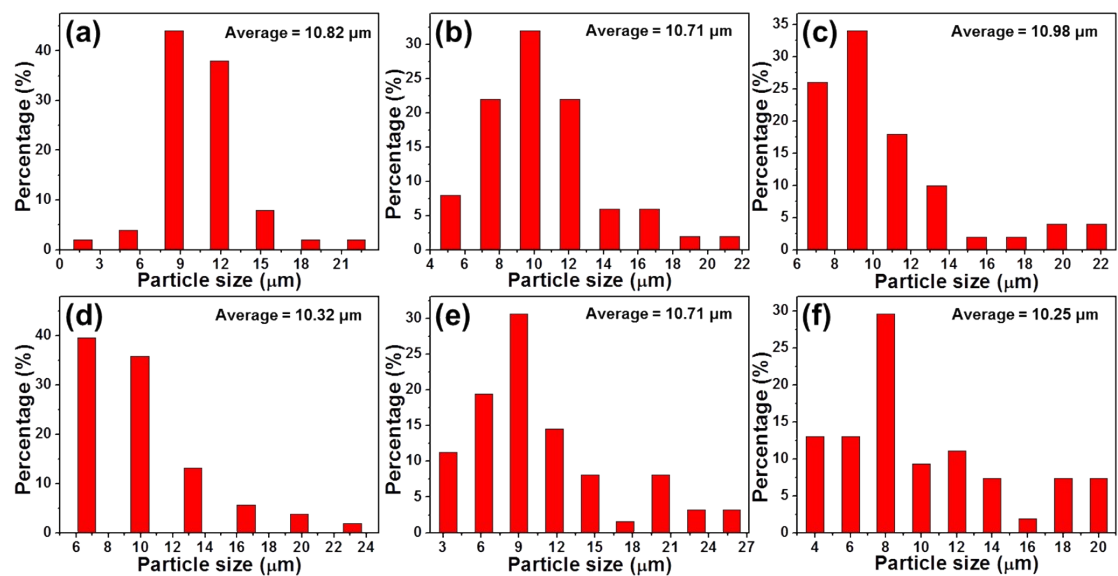


Figure S3. Particle size distribution $\text{LiSrVO}_4:x\text{Sm}^{3+}$ (a) $x = 0.00$, (b) $x = 0.005$, (c) $x = 0.01$, (d) $x = 0.03$, (e) $x = 0.05$ and (f) $x = 0.07$ phosphors.

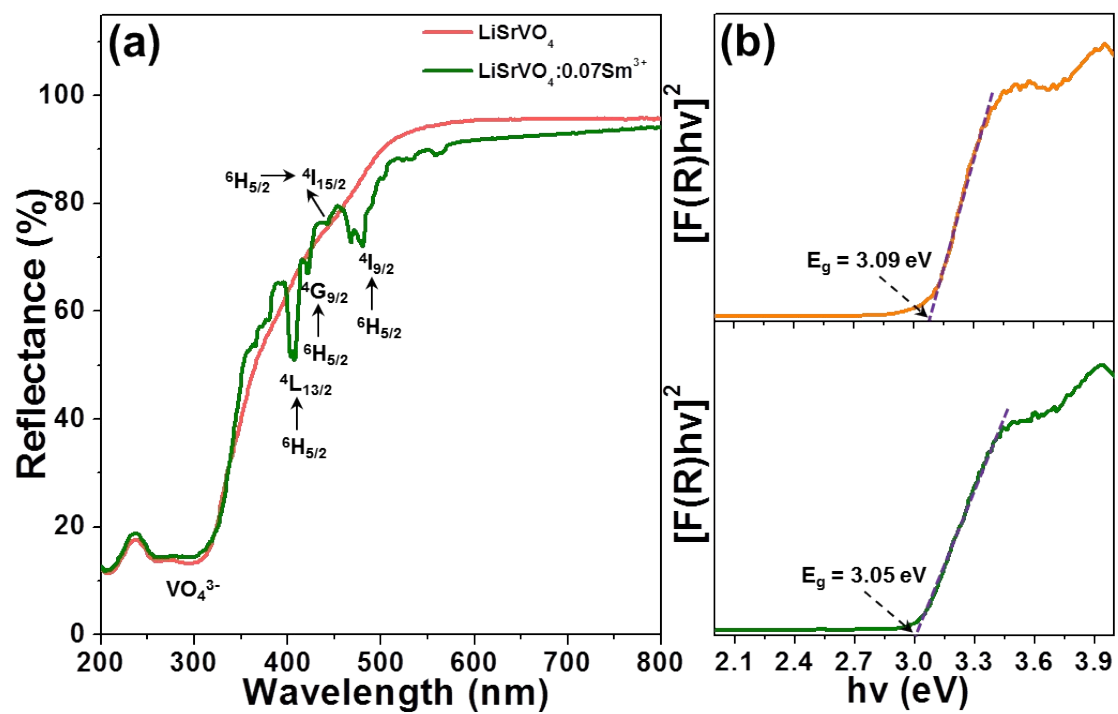


Figure S4. (a) UV-Vis DRS spectra of the LiSrVO_4 and $\text{LiSrVO}_4:0.01\text{Sm}^{3+}$ phosphors. The determination of the optical band gap of (b) LiSrVO_4 and (c) $\text{LiSrVO}_4:0.01\text{Sm}^{3+}$ phosphors.

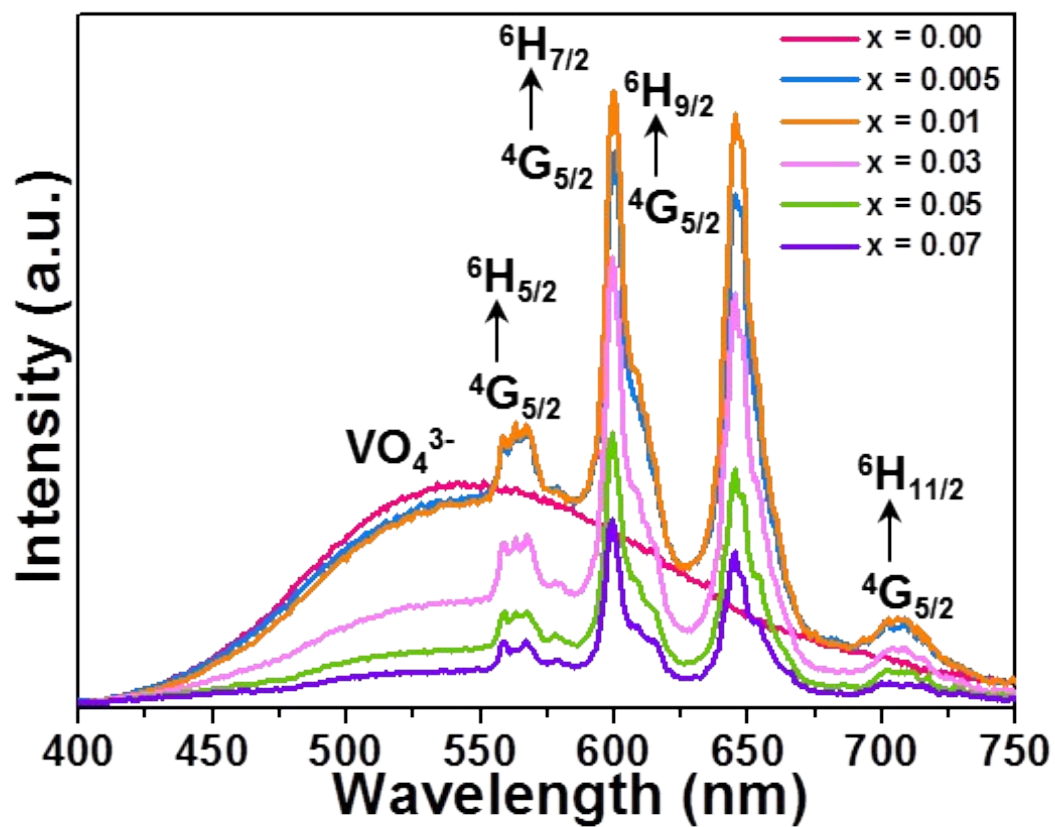


Figure S5. Emission spectra of the $\text{LiSrVO}_4:\text{xSm}^{3+}$ phosphors with different doping concentrations excited at 343 nm.

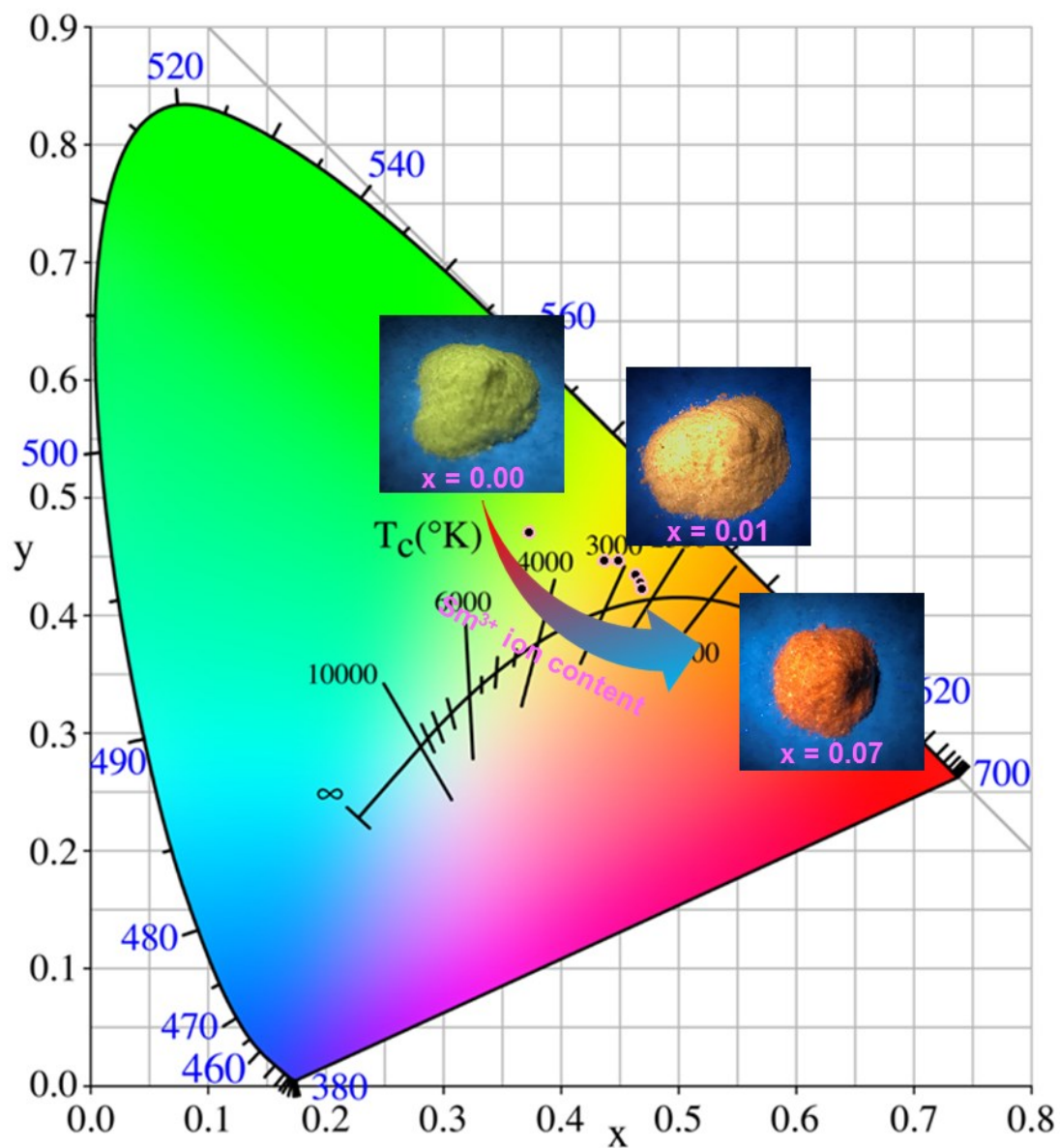


Figure S6. CIE chromaticity diagram of the $\text{LiSrVO}_4:x\text{Sm}^{3+}$ phosphors. Inset shows the optical images of the resultant phosphors upon 365 nm lamp irradiation.

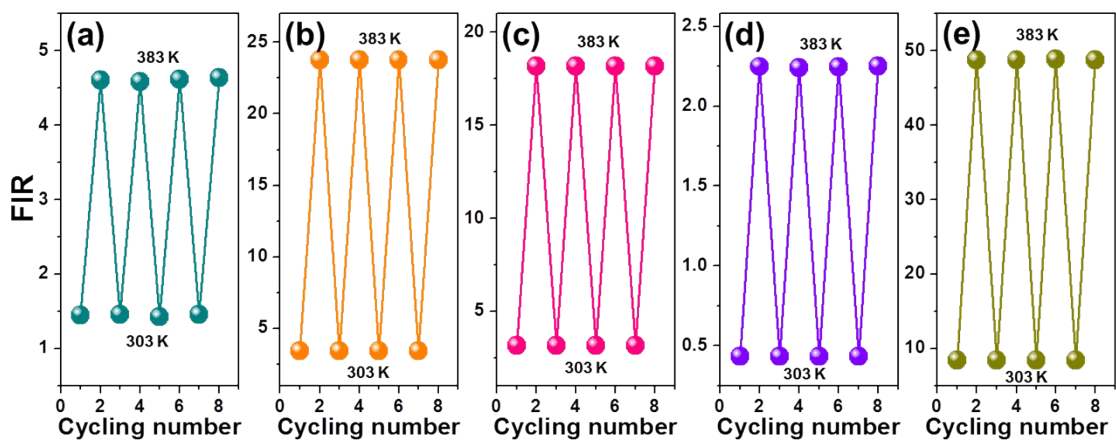


Figure S7. Temperature-induced switching of FIR values of (a) ${}^6\text{H}_{5/2}/\text{VO}_4^{3-}$, (b) ${}^6\text{H}_{7/2}/\text{VO}_4^{3-}$, (c) ${}^6\text{H}_{9/2}/\text{VO}_4^{3-}$, (d) ${}^6\text{H}_{11/2}/\text{VO}_4^{3-}$ and (e) total integrated ${}^6\text{H}_{11/2}/\text{VO}_4^{3-}$ of $\text{LiSrVO}_4:0.01\text{Sm}^{3+}$ phosphors in the range of 303-383 K.

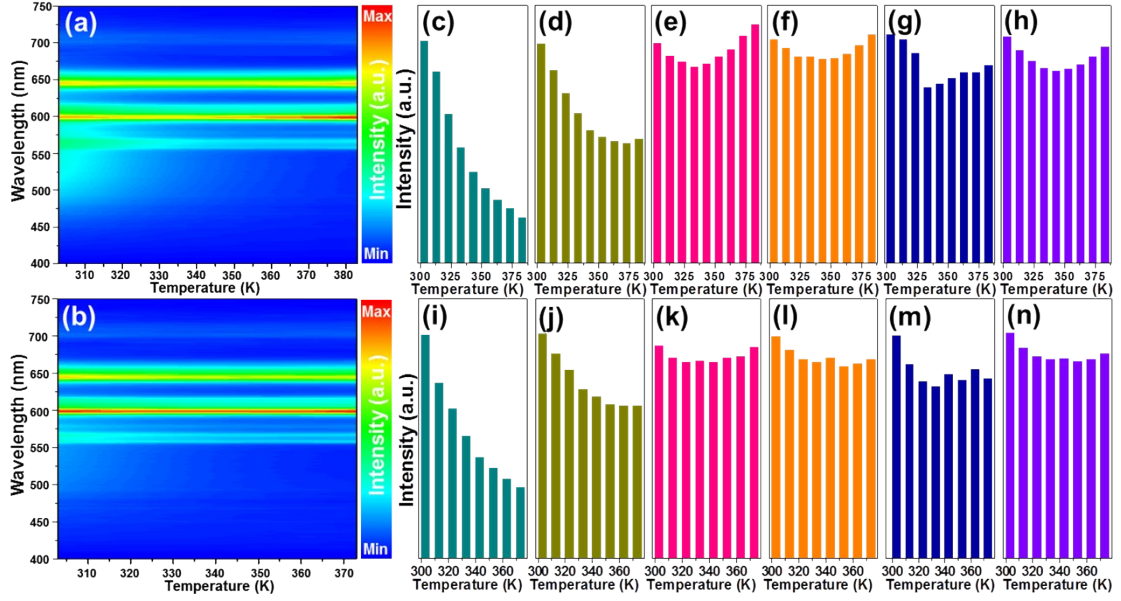


Figure S8. Contour mapping of thermal evolution emission spectra of (a) the $\text{LiSrVO}_4:0.005\text{Sm}^{3+}$ and (b) $\text{LiSrVO}_4:0.05\text{Sm}^{3+}$ phosphors. Temperature dependent emission intensities of (c) VO_4^{3-} group, (d) ${}^4\text{G}_{5/2} \rightarrow {}^6\text{H}_{5/2}$ transition, (e) ${}^4\text{G}_{5/2} \rightarrow {}^6\text{H}_{7/2}$ transition, (f) ${}^4\text{G}_{5/2} \rightarrow {}^6\text{H}_{9/2}$ transition, (g) ${}^4\text{G}_{5/2} \rightarrow {}^6\text{H}_{11/2}$ transition and (h) total integrated ${}^4\text{G}_{5/2} \rightarrow {}^6\text{H}_J$ ($J = 5/2, 7/2, 9/2, 11/2$) transitions. Temperature dependent emission intensities of (i) VO_4^{3-} group, (j) ${}^4\text{G}_{5/2} \rightarrow {}^6\text{H}_{5/2}$ transition, (k) ${}^4\text{G}_{5/2} \rightarrow {}^6\text{H}_{7/2}$ transition, (l) ${}^4\text{G}_{5/2} \rightarrow {}^6\text{H}_{9/2}$ transition, (m) ${}^4\text{G}_{5/2} \rightarrow {}^6\text{H}_{11/2}$ transition and (n) total integrated ${}^4\text{G}_{5/2} \rightarrow {}^6\text{H}_J$ ($J = 5/2, 7/2, 9/2, 11/2$) transitions.

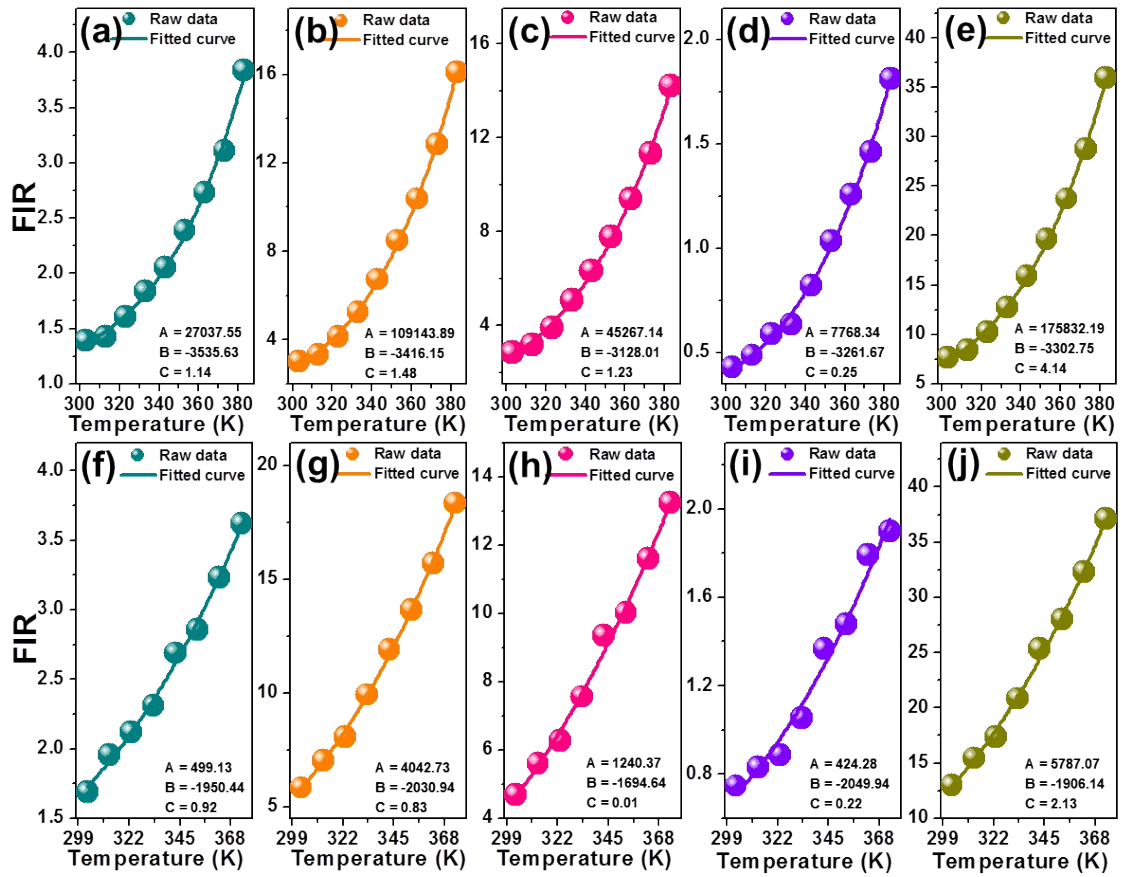


Figure S9. Temperature dependent FIR values of (a) ${}^6\text{H}_{5/2}/\text{VO}_4^{3-}$, (b) ${}^6\text{H}_{7/2}/\text{VO}_4^{3-}$, (c) ${}^6\text{H}_{9/2}/\text{VO}_4^{3-}$, (d) ${}^6\text{H}_{11/2}/\text{VO}_4^{3-}$ and (e) total integrated ${}^6\text{H}_{11/2}/\text{VO}_4^{3-}$ of $\text{LiSrVO}_4:0.005\text{Sm}^{3+}$ phosphors. Temperature dependent FIR values of (f) ${}^6\text{H}_{5/2}/\text{VO}_4^{3-}$, (g) ${}^6\text{H}_{7/2}/\text{VO}_4^{3-}$, (h) ${}^6\text{H}_{9/2}/\text{VO}_4^{3-}$, (i) ${}^6\text{H}_{11/2}/\text{VO}_4^{3-}$ and (j) total integrated ${}^6\text{H}_{11/2}/\text{VO}_4^{3-}$ of $\text{LiSrVO}_4:0.05\text{Sm}^{3+}$ phosphors.